Available online at www.sciencedirect.com
SCIENCE DIRECT®
PERGAMON
Continental Shelf Research 23 (2003) 777–800
CONTINENTAL SHELF RESEARCH
www.elsevier.com/locate/csr

West Florida shelf circulation and temperature budget for the 1998 fall transition

Ruoying He*, Robert H. Weisberg

College of Marine Sciences, University of South Florida, 140 7th Ave. South, St. Petersburg, Florida 33701, USA

Received 7 May 2002; accepted 27 January 2003

Abstract

Mid-latitude continental shelves undergo a fall transition as the net heat flux changes from warming to cooling. Using in situ data and a numerical model we investigate the circulation on the west Florida shelf (WFS) for the fall transition of 1998. The model is a regional adaptation of the primitive equation, Princeton Ocean Model forced by NCEP reanalysis wind, air pressure, and heat flux fields, plus river inflows. After comparison with observations the model is used to draw inferences on the seasonal and synoptic scale features of the shelf circulation. By running twin experiments, one without and the other with an idealized Loop Current (LC), we explore the relative importance of local versus deep-ocean forcing. We find that local forcing largely controls the inner-shelf circulation, including changes from the Florida Panhandle in the north to regions farther south. The effects of the LC in fall 1998 are to reinforce the mid-shelf currents and to increase the across-shelf transports in the bottom Ekman layer, thereby accentuating the shoreward transport of cold, nutrient rich water of deep-ocean origin. A three-dimensional analysis of the temperature budget reveals that surface heat flux largely controls both the seasonal and synoptic scale temperature variations. Surface cooling leads to convective mixing that rapidly alters temperature gradients. One interesting consequence is that upwelling can result in near-shore warming as warmer offshore waters are advected landward. The temperature balances on the shelf are complex and fully three-dimensional.

Keywords: West Florida shelf; Observations; Circulation modeling; Temperature budget

1. Introduction

The circulation on the continental shelf controls the exchange of materials between the coast and deep-ocean. The circulation is therefore a primary determinant of shelf ecology. Influenced by both local (surface winds, air pressure, surface buoyancy fluxes, and river inflows) and deep-ocean (boundary currents and eddies) forcing, the shelf circulation is dynamically linked to the varying water properties, particularly the temperature which exerts the primary control on density. Continental shelf temperature budgets are known to vary with location. Lentz (1987), Lentz and Chapman (1989) and Dever and Lentz (1994) studied the temperature variations of the northern California shelf and found the balance to be primarily two-dimensional (controlled by

*Corresponding author. Tel.: +1-727-553-1627; fax: +1-727-553-1189.
E-mail address: ruoying@marine.usf.edu (R. He).

0278-4343/03/$ - see front matter
doi:10.1016/S0278-4343(03)00028-1

across-shelf and surface heat fluxes), independent of season. With an array of instruments deployed to the north of Cape Hatteras from August through November 1994, Austin (1999) found distinctive seasonal variations in the temperature balance of the North Carolina shelf that are closely linked to water column stratification. From May to August (under stratified conditions), across-shelf advection controls the vertically integrated temperature budget. From October to March (under well-mixed conditions), surface heat flux and along-shelf advection dominate the variations. He and Weisberg (2002a), hereafter referred to as HW02, describe the temperature budget on West Florida Shelf (WFS) during the spring transition of 1999. The thermodynamics are fully three-dimensional and when vertically integrated the surface heat flux and the ocean circulation control the seasonal and synoptic scale variability, respectively.

Opposite from the spring transition, which begins when the net surface heat flux changes from cooling to warming and the water column stratifies, the fall transition begins when the net surface heat flux changes from warming to cooling and the water column destratifies. How the evolution of the three-dimensional temperature structure of the WFS differs between the spring and fall transitions is the main topic of the present paper. To explore this question, we first need to understand the shelf circulation and how local and deep-ocean forcing affect the hydrodynamics and thermodynamics.

We follow the approach of HW02 in which we combine in situ data with an adaptation of the primitive equation, Princeton Ocean Model (POM) of Blumberg and Mellor (1987). The model is forced by National Center for Environment Prediction (NCEP) reanalysis wind, air pressure, and net surface heat flux fields, plus river inflows to study the seasonal circulation and temperature budget for September 1st to November 30th, 1998. By comparing twin experiments, one independent of the Gulf of Mexico Loop Current (LC) and the other including an idealized version of the LC, we also investigate the relative importance of local versus deep-ocean forcing in determining the shelf circulation and temperature budget for the fall 1998 transition.

The model and forcing fields are described in Section 2. Section 3 presents the twin experiments and compares the model results with observations. The model is then used in Section 4 to describe the seasonal mean circulation and the corresponding temperature and salinity fields. Section 5 presents a term-by-term analysis of the three-dimensional temperature budget. Section 6 provides a summary and conclusions.

2. Model and forcing fields

2.1. Model

In parallel with HW02 the domain (Fig. 1) extends from the Florida Keys to the Mississippi River delta, and it has one open boundary arcing in between. An orthogonal curvilinear grid is used in the horizontal with resolution varying from about 2 km near the coast to 6 km near the open boundary. A sigma coordinate is used in the vertical with 21 layers non-uniformly distributed to better resolve the near-surface and near-bottom frictional boundary layers. Horizontal diffusivities are parameterized according to Smagorinsky (1963) with a dimensionless coefficient of 0.2. Vertical diffusivities follow the Mellor and Yamada (1982) level 2.5 closure scheme, and bottom stress follows a quadratic law using a variable drag coefficient with a minimum value of 0.0025. A mode splitting technique is employed with external and internal time steps of 12 and 360 s, respectively.

The model is initialized at rest with horizontally uniform stratification. Above and below 200 m stratification is based on temperature and salinity observed in a September 1998 hydrographic survey and climatology, respectively. From this initial zero-baroclinicity state the model spins up rapidly, generating baroclinicity in balance with the wind, air pressure, and buoyancy forcing as justified in HW02.

Tidal forcing is excluded since, with tidal currents of only a few $cm\,s^{-1}$, the related tidal mixing is weak in comparison with other sources for mixing. A WFS tidal analysis along with

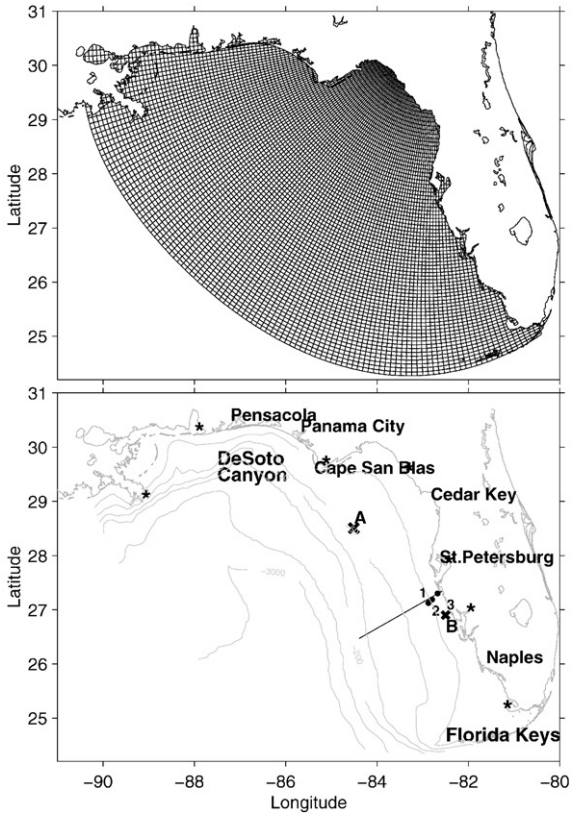

Fig. 1. The regional model grid and bathymetry (upper panels) and observational station locations (lower panels). Sea level comparisons are with Florida tide gauges at Pensacola, Apalachicola, St. Petersburg, and Naples. Velocity comparisons are with acoustic Doppler current profiles from instruments moored at 25, 20 and 10 m isobath (1–3). Temperature budget is diagnosed at station A, B. Seasonal mean temperature budget is diagnosed along a transect off Sarasota, FL. Along the coast from west to east, seven major rivers indicated by stars are: Mississippi, Mobile, Apalachicola, Suwannee, Hillsborough, Peace, and Shark rivers.

discussions on tidal mixing efficacy is given in He and Weisberg (2002b).

2.2. Atmospheric forcing

The relatively coarse resolution ($2.5^\circ \times 2.5^\circ$) NCEP wind, air pressure, and surface heat flux fields are interpolated onto the model grid. Whereas the coarse wind and pressure fields are representative of nature, the surface heat flux field does not match the spatial scales of sea surface temperature (SST) variability. We attempt to remedy this by applying a surface heat flux correction that relaxes the modeled SST toward a monthly mean SST analysis derived from satellite images (e.g., Ezer and Mellor, 1992; Chu et al., 1999). This procedure (as in HW02) facilitates realistic baroclinic structures since the density perturbations originating at the surface are mixed vertically through the model's turbulence closure scheme.

2.3. Lateral boundary forcing

Examination of TOPEX/POSEIDON (T/P) time series indicates an impact by the LC on the southwest corner of the WFS in fall 1998. LC impacts on the WFS and their effects on the shelf circulation are the subjects of recent studies by Hetland et al. (1999), Meyers et al. (2000), He and Weisberg (2003) and Weisberg and He (2003). Hetland et al. (1999) hypothesize that LC impacts on the southwest corner can set currents in motion on the WFS by virtue of isobath converge there. Pressure perturbations at the point of isobath convergence can propagate along isobath into the shelf interior, thereby affecting the shelf circulation. Weisberg and He (2003) confirm this hypothesis using the He and Weisberg (2003) technique for including an idealized LC in the model domain. The latter paper also shows that LC impacts occurring farther north along the shelf-break do not set shelf currents in motion, consistent with the findings of Meyers et al. (2000). Here we apply the same technique in a twin experiment to determine the relative importance of local versus LC forcing during the fall 1998 seasonal transition. A LC impact is mimicked by imposing a Gaussian shaped sea surface height perturbation along the open boundary west of the Florida Keys. Geostrophic inflows and outflows occur on either side, and the ensuing current freely evolves within the model domain. The mode splitting technique by which all of the vertically integrated transport is contained in the barotropic mode ensures a rapid baroclinic adjustment near the open boundary. We use T/P data to estimate the location and magnitude of the pressure perturbation, and for simplicity (and lack of data)

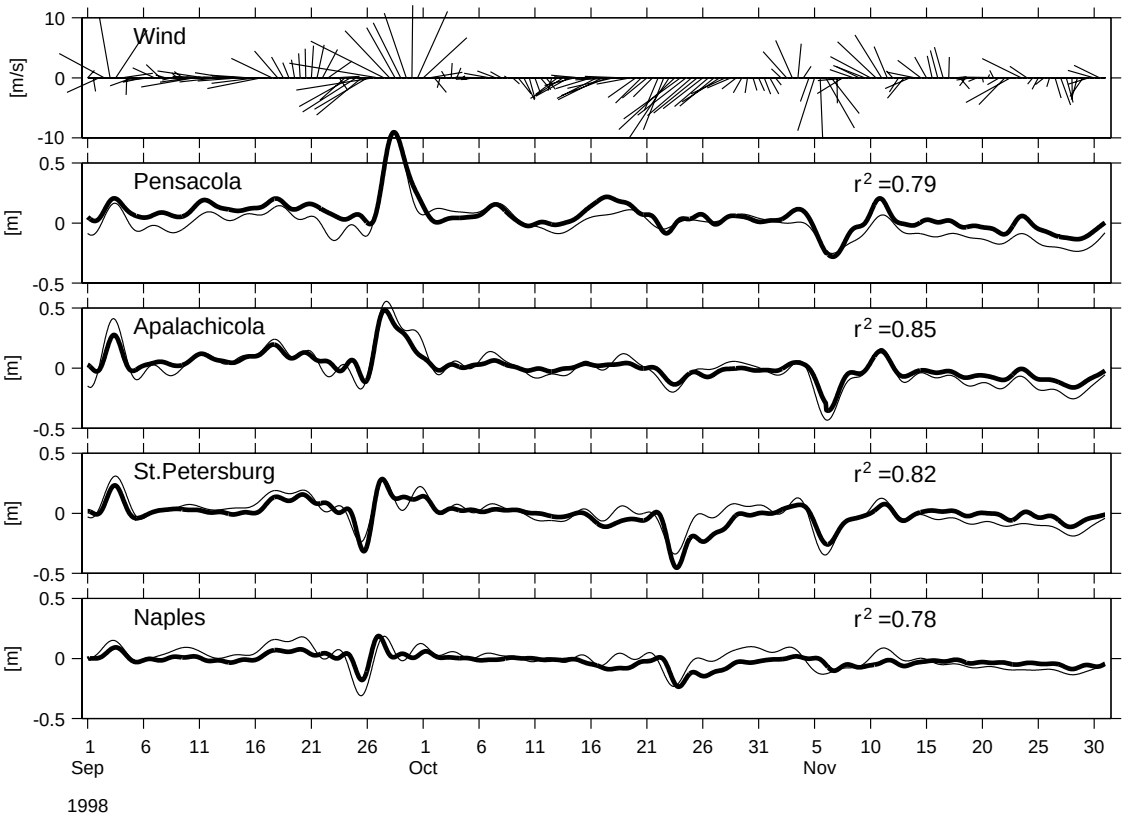

Fig. 2. Comparisons between modeled (bold lines) and observed (thin lines) sea level at Pensacola, Apalachicola, St. Petersburg, and Naples as quantified by squared correlation long with NCEP wind velocity sampled at station A. Modeled results are from Case I.

the pressure perturbation is held constant over the three-month simulation. Other than the imposed pressure perturbation the open boundary is treated with an (Orlanski, 1976) radiation boundary condition.

Seven major rivers (Fig. 1) are included: the Mississippi, Mobile, Apalachicola, Suwannee, Hillsborough, Peace, and Shark rivers. Interpolated monthly mean fresh water mass fluxes are input to the top sigma level at the grid cells closest to the rivers' locations using the technique of Kourafalou et al. (1996) (also see Pullen, 2000).

3. Model and data comparison

This section compares the model twin experiments, one with local forcing only (Case I) and the other with both local and idealized LC forcing (Case II), against in situ sea level and velocity data.

3.1. Sea level

Since the model is forced without tides, all of the model and data comparisons are shown after low-pass filtering to exclude tidal and inertial period oscillations. Case I sea level comparisons are given in Fig. 2 at four different NOAA tide-gauge stations from Pensacola in the northwest to Naples in the southeast. Three hurricanes transited the model domain in fall 1998: Earl (August 31 to September 3), Georges (September 16–29), and Mitch (October 22 to November 5). The storm surge simulations for these and other synoptic scale events are reasonably good, with squared correlation values of around 0.8 at all stations.

Case II comparisons (not shown) are similar to Case I, essentially in agreement with Marmorino (1982) who found that the coastal sea level response to winds is insensitive to the LC configuration near the shelf-break. We conclude that coastal sea level variability in fall 1998 is primarily in response to local, shelf-wide forcing.

3.2. Currents

Comparisons are made between modeled and observed velocity vector time series at the 25, 20, and 10 m isobaths (moorings NA2, EC4, and EC5, respectively, as shown in Fig. 1). The Case I comparisons are given in Figs. 3–5. The observations are from moored Acoustic Doppler Current Profilers (ADCP), and comparisons are provided at three different depths: near-surface, mid-water column, and near-bottom. We quantify these comparisons using a complex correlation analysis (i.e., Kundu, 1976; HW02), the results of which are given as two sets of numbers on each plot. The left-hand sets are the seasonal mean east and north velocity components for each vector time series. The right-hand sets are the squared correlation coefficients, the relative orientation angles (measured anti-clockwise), and the regression coefficients between the modeled and the observed velocity vectors. Like sea level, the modeled and observed currents also compare reasonable well. At all three stations and depths, the squared correlation coefficients range between about 0.59 and 0.78, and the orientations agree to between about -3° to $+12^\circ$. Disparities are seen in the time series on an event-by-event basis. First, the model fails to pick up some of the reversals in the observed currents. Second, the regression coefficients show that the model underestimates the amplitude of observed velocity fluctuation by 20–50%. Such deficiencies may result from the low resolution of NCEP reanalysis fields that exclude smaller-scale coastal boundary layer structures in the winds. Coarse resolution problems are further exacerbated by smoothing to interpolate the reanalysis fields onto the model grid. Nevertheless, the model captures the general features of the observations and gets the sense of the rotation correct in both surface and bottom Ekman layers. Presumably, improved forcing functions will lead to improved quantitative comparison metrics.

As with sea level, the Case II comparisons (not shown) are similar to those of Case I. Adding the LC provides only subtle differences in the modeled currents of the inner-shelf. As shown for the 25 m isobath in Fig. 6 the modeled southeastward currents in Case II are a little stronger than in Case I, but the synoptic scale variability between the two cases are nearly the same. These results are summarized in Fig. 7 where seasonal mean velocity vectors and seasonal mean velocity hodograph ellipses are provided at mid-depth for the observations and the model results for both cases. We may conclude that the inner-shelf currents were primarily in response to local forcing in fall 1998.

Velocity measurements at deeper isobaths are not available. Based on our inner-shelf results and the spring/summer period findings of Weisberg and He (2003) when deeper measurements are available, we now use the model to draw inferences on the mid- to outer-shelf circulation.

4. Modeled seasonal mean circulation

4.1. Circulation fields

The seasonal mean circulation fields, obtained by averaging the model flow vectors from September 1st to November 30th, are presented in Figs. 8 and 9 for Cases I and II, respectively. Each figure shows the depth-average, near-surface (sigma layer 2), mid-depth (sigma layer 10), and near-bottom (sigma layer 20) currents. Three-dimensionality arises by geometrical factors such as blocking by the Florida Keys, coastline changes from the Big Bend to the Panhandle, near-shore penetration of deep isobaths at DeSoto Canyon, and by the effects of baroclinicity and surface and bottom Ekman layers. The mid-depth and depth-average fields are similar, and they show the general nature of the mean currents exclusive of the Ekman layer effects. The near-surface (near-bottom) currents are larger (smaller) and these differences in magnitude are accommodated for illustration purposes by scale changes as noted.

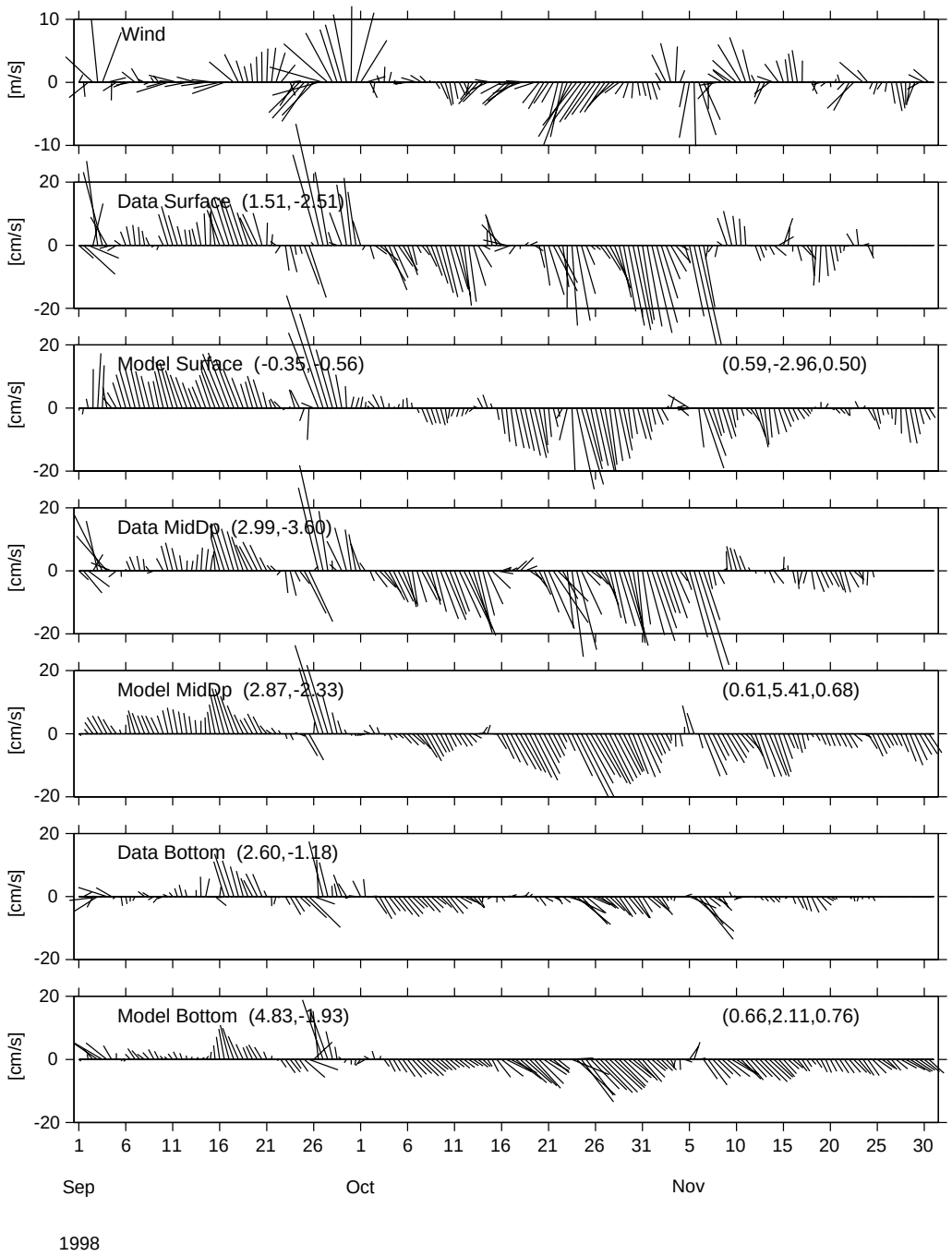

Fig. 3. Comparisons between modeled and observed currents at the 25 m isobath (mooring NA2) sampled at surface, mid-depth and near the bottom, along with the NCEP wind sampled at Station A. Each vector current time series is accompanied by its seasonal mean east and north velocity components (left-hand couplet), and each model/data comparison is quantified by its squared complex correlation coefficient, phase angle (or angular deviation of the model vectors from the data vector measured counterclockwise), and regression coefficient (right-hand triplet) Modeled results are from Case I.

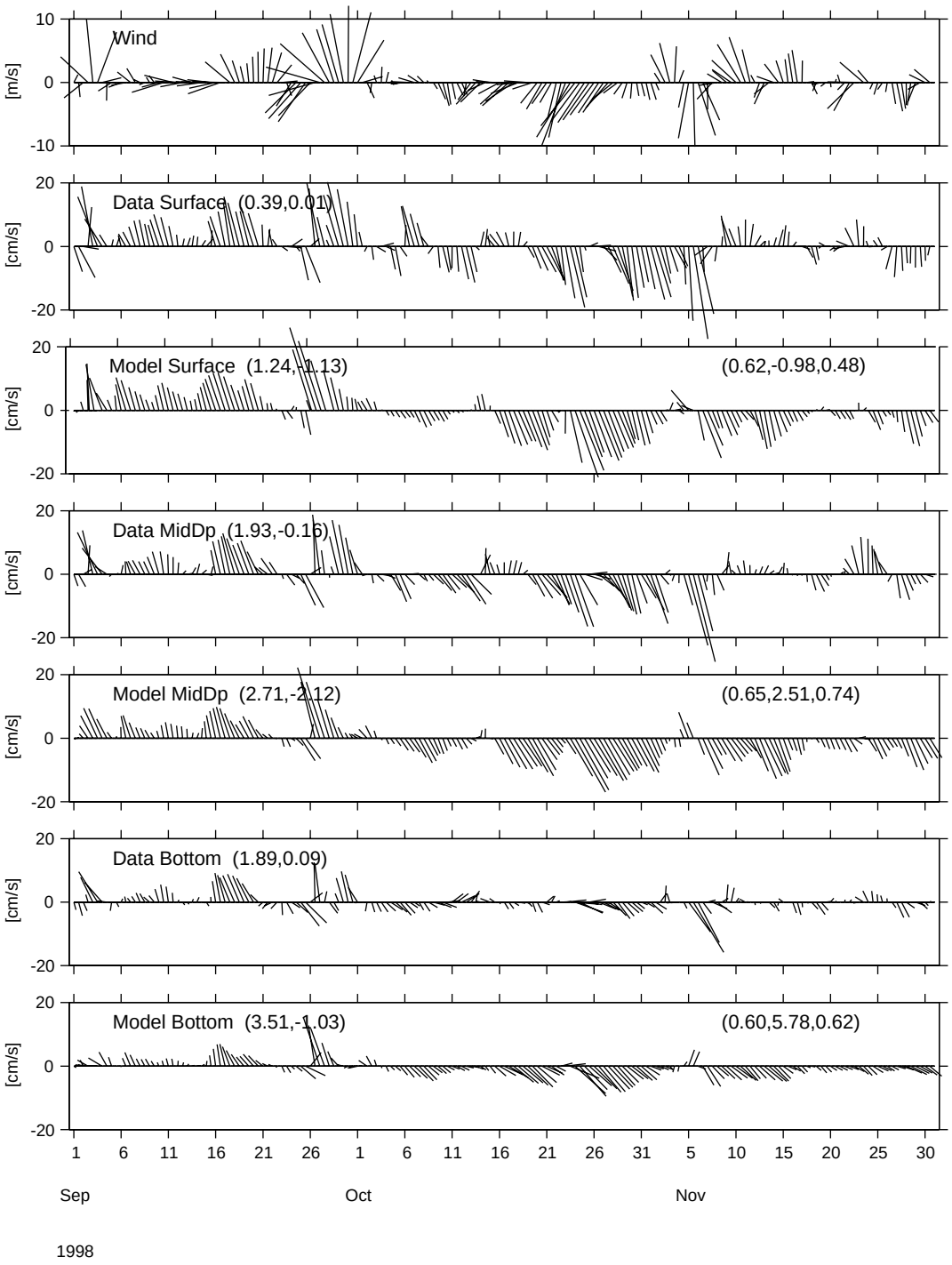

Fig. 4. Comparisons between modeled and observed currents at the 20 m isobath (mooring EC4) sampled at surface, mid-depth and near bottom along with the NCEP wind velocity sampled at Station A. Quantitative comparisons are as in Fig. 3. Modeled results are from Case I.

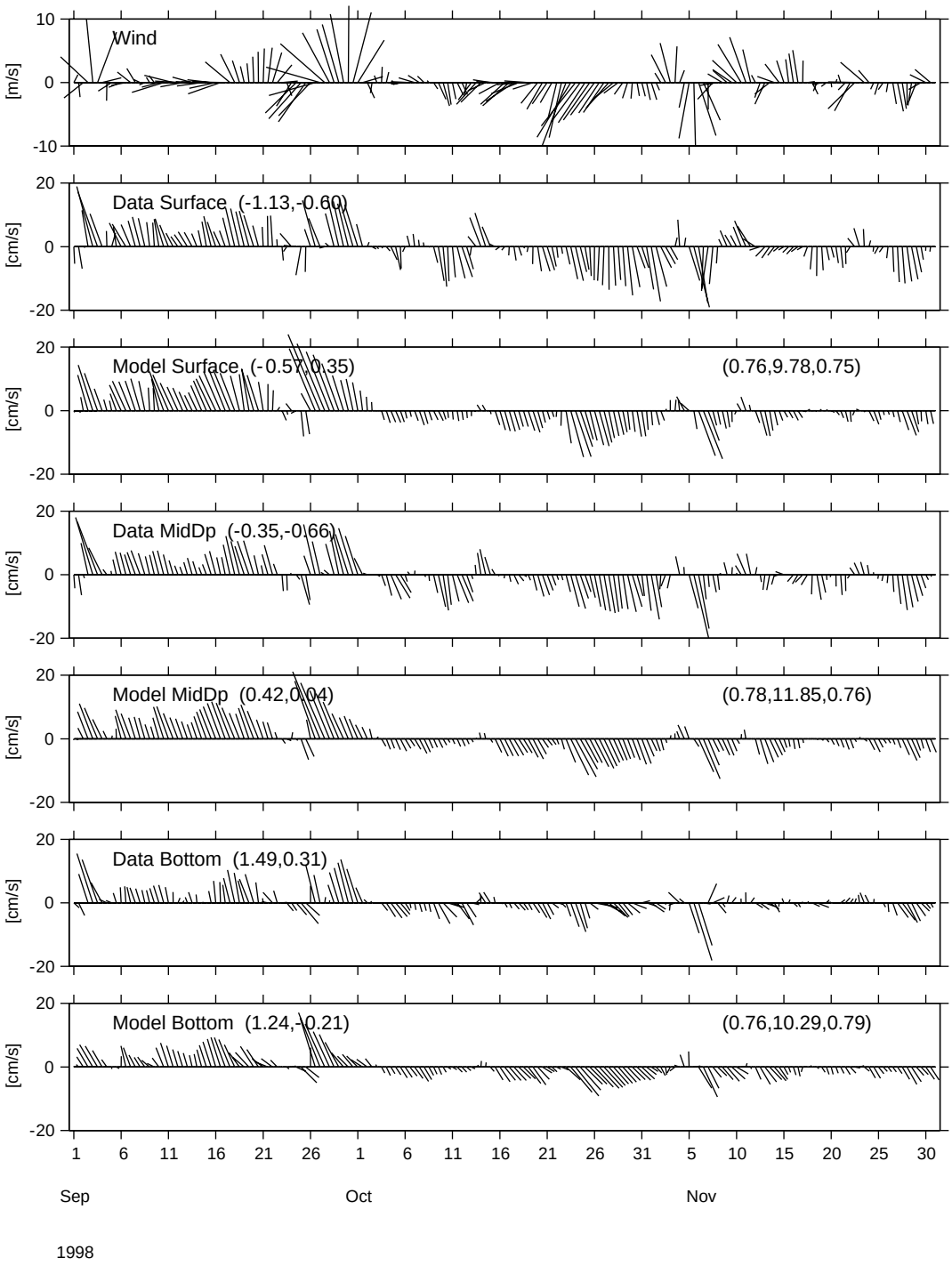

Fig. 5. Comparisons between modeled and observed currents at the 10 m isobath (mooring EC5) sampled at surface, mid-depth and near bottom along with the NCEP wind velocity sampled at Station A. Quantitative comparisons are as in Fig. 3. Modeled results are from Case I.

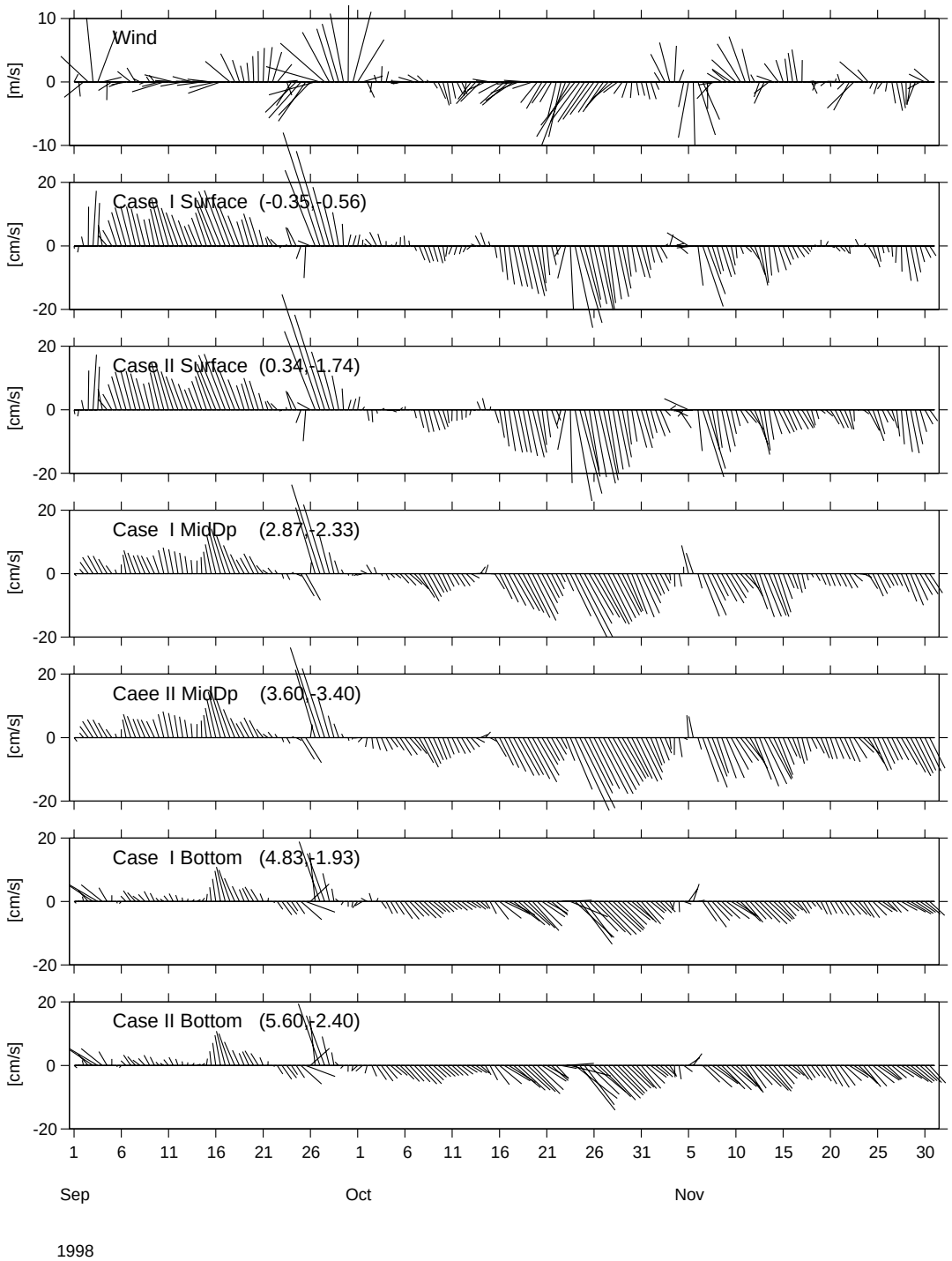

Fig. 6. Comparisons between modeled currents of Cases I and II at the 25 m isobath (mooring NA2) sampled at surface, mid-depth and near bottom along with the NCEP wind velocity sampled at Station A.

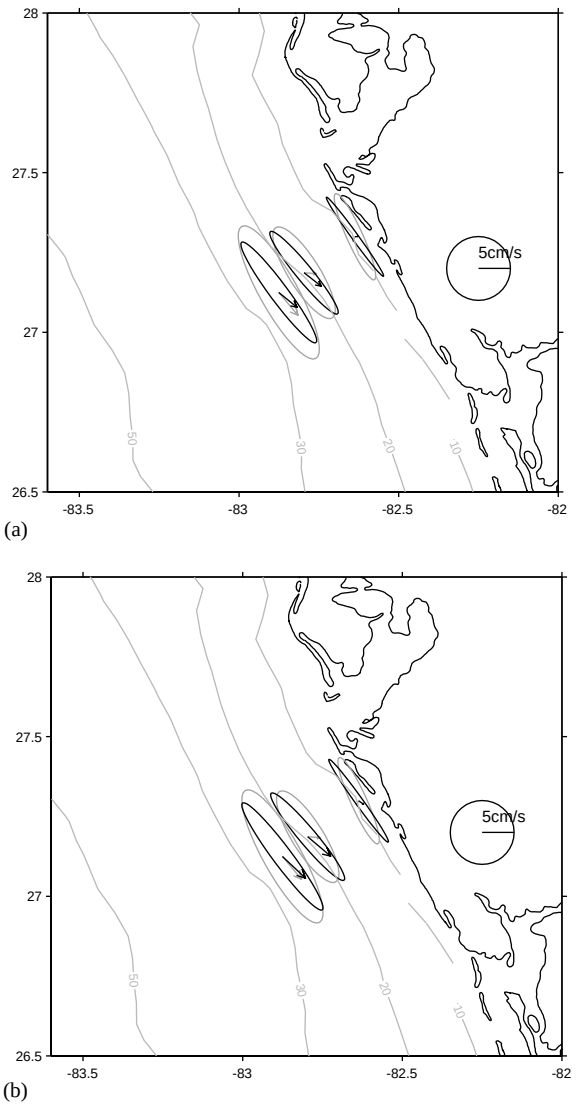

Fig. 7. Comparisons between modeled (bold) and observed (thin) seasonal mean velocity vectors and hodograph ellipses at mid-depth for all three mooring locations on the WFS between 25 and 10 m isobath. Upper (lower) panel is for Case I (Case II).

Commonality exists for some of features in both cases. Near-shore, the depth-average and mid-depth currents show a divergence about the Big Bend region in which the currents flow westward west of Cape San Blas and southward between Tampa Bay and the Florida Keys. At the shelf-break these currents tend to be southward. The near-surface and near-bottom currents are different. Near-surface we see a northward jet at the shelf-break that is continuous with the westward flows along the Panhandle and the Florida Keys. Near-shore off Tampa Bay (Florida's west coast) we see an offshore-directed flow. All of these surface features are attributable to a general easterly wind pattern on average (Fig. 10). Near-bottom off Florida's west coast we see a shoreward directed across-shelf flow pattern in the bottom Ekman layer which is consistent with the southward flow at mid-depth. This upwelling favorable circulation appears to be a general feature of the fall season that appears (with differing amplitude and phase) each year in our extended observational records. Water approaches the coast at depth from the north, upwells near-shore, and then flows southward and away from the coast at the surface. An upwelling case study for a specific synoptic scale event is described by Weisberg et al. (2000), and these simple Ekman-geostrophic adjustment concepts coupled with the WFS geometry account for the absence of surface drifters near-shore south of Tampa Bay as described by Yang et al., (1999). In contrast with Florida's west coast, the bifurcation of the depth-average currents in the Big Bend results in a downwelling favorable regime along the Florida Panhandle coast. Thus the coastline and isobath geometry relative to the seasonal wind patterns largely dictates the structure of the regional flow fields.

Along with commonality there are also distinct differences between the two cases, particularly over the mid- to outer-shelf regions. With the LC influence (Fig. 9), we see a broader and stronger southward mid-shelf current along with a broader and stronger across-shelf flow pattern in the bottom Ekman layer everywhere south of Cape San Blas. We attribute this to the constructive interference that occurs between the LC and local forcing effects over this portion of the model domain. In contrast we see destructive interference along the Panhandle coast west of Cape San Blas. The result is a diminution of the downwelling favorable circulation there. While remote, we find that the impact of the LC (on relatively shallow isobaths at the shelf-break west of the Florida Keys) is propagated throughout the entire model

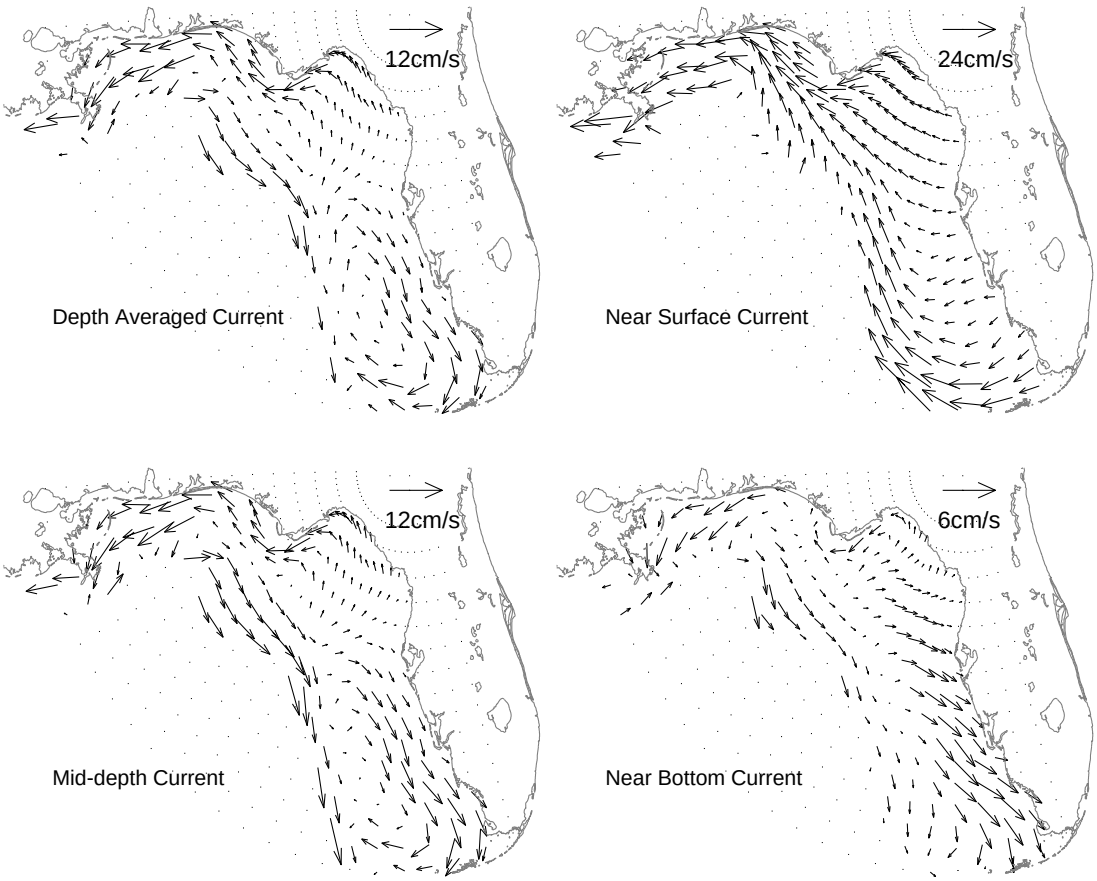

Fig. 8. Modeled (Case I) seasonal mean velocity vectors for the depth averaged and near surface, mid-depth, and near bottom sigma levels, $k = 2$, 10, 20, respectively.

domain to the Mississippi River delta. This occurs quickly through the anticlockwise propagation of continental shelf waves (e.g., Gill, 1982, p. 408), which, with celerity of order m s^{-1}, can transit the model domain in a matter of days.

Weisberg et al. (1996) hypothesized that the evolution of the seasonal mean fields involves both wind and surface heat flux forcing. HW02 demonstrated this for the spring 1999 transition, and similar factors come to play in fall, the difference in fall being that the net surface heat flux changes from warming to cooling. Figs. 11 and 12 provide the September, October, November, and seasonal mean depth-average velocity fields for Cases I and II, respectively. Beginning in September, and consistent with the mean wind field (Fig. 10), we see a northward directed current with largest magnitude near the coast. As the winds switch from southeasterly to northeasterly in October the currents change markedly, in part due to heat flux. Summer months are when the near-shore temperatures are highest and the baroclinic geostrophic circulation tends to be northward and downwelling favorable. Hence the September currents show largest magnitude near-shore where the wind and buoyancy-induced circulations add constructively. By October the near-shore waters are cooled by the net surface heat flux, which reverses the sign of the thermal wind and causes a constructive interference with the now slightly upwelling favorable winds. By November the on-shore-directed density gradient

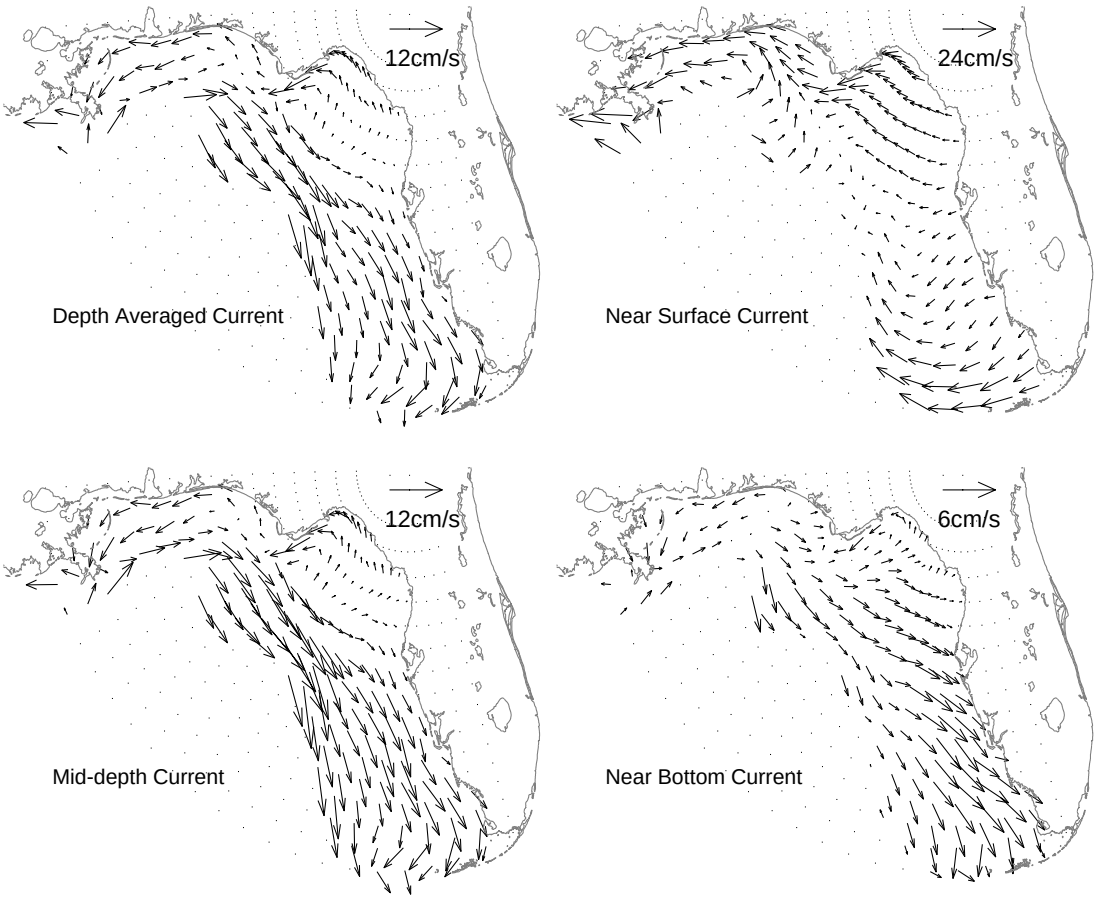

Fig. 9. Modeled (Case II) seasonal mean velocity vectors for the depth averaged and near surface, mid-depth, and near bottom sigma levels, $k = 2$, 10, 20, respectively.

is positioned closer to the shelf-break so the near-shore currents are primarily wind-driven, whereas the shelf-break currents are largely buoyancy driven. Hence the region of maximum current sidles seaward with the region of maximum density gradient over the fall season march. Moreover, the current direction changes from northward to southward as the net surface heat flux reverses the density gradient from seaward to landward.

Case II shows (Fig. 12) that the LC provides additional constructive/destructive interference as previously described with respect to Figs. 8 and 9. Flows directed from the Mississippi River region toward the Florida Keys are increased, whereas flows in the opposite direction are decreased. As a result there is a shoreward translation of the region of southward directed currents going from the Big Bend region to points farther south. Under LC influence the entire shelf south of the Big Bend shows stronger southward-directed currents than Case I, and this has a profound effect upon across-shelf transport as we will show next.

4.2. Lagrangian trajectories

The bottom Ekman layer is a major conveyance for the across-shelf transport of materials on the WFS (Weisberg et al., 2001; Weisberg and He, 2003). Such bottom Ekman layer transport, further amplified by LC effects in spring-fall 1998, accounts for the cold, nutrient-rich water of deep-ocean origin reported by Nowlin et al.

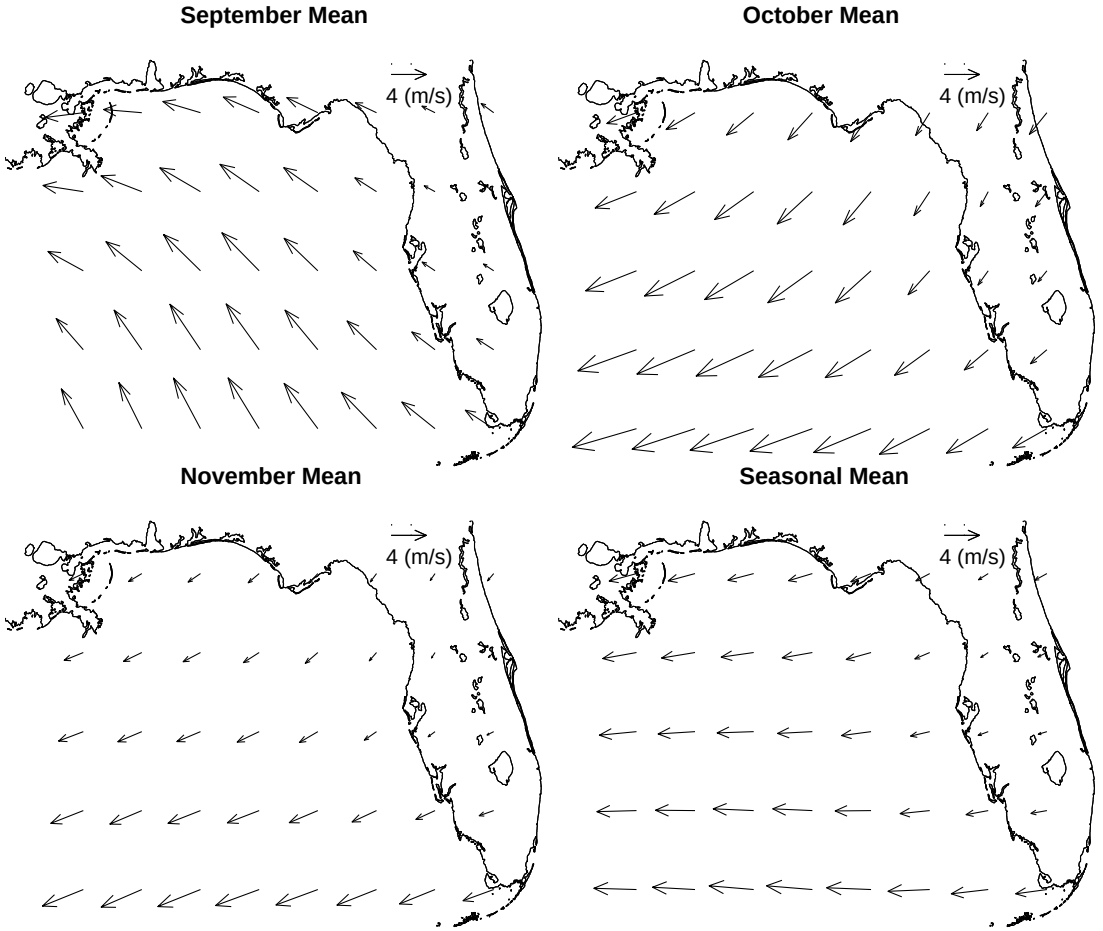

Fig. 10. Monthly (September, October and November) and seasonal mean surface wind fields.

(2000) and Walsh et al. (2003). To illustrate this finding, we show Lagrangian trajectories for neutrally buoyant particles advected by the modeled three-dimensional flow fields for Cases I and II. Fig. 13 shows trajectories for particles released on September 1st in the near-bottom sigma layer 18 along the 25, 50, and 100 m isobaths. Particles released at the 25 m iosbath all find their way to the near-shore zone in either case. From the 50 m isobath we see some assistance by the LC-induced flows, especially from positions originating within the Big Bend. Constructive interference between locally forced and LC-induced flows within the water column increases the bottom Ekman layer responses and hence the across-shelf transports. This effect is most evident in the 100 m isobath panels where across-shelf transports are only evident under the influence of the LC. Thus the delivery of cold, nutrient-rich waters from the shelf-break to the near-shore in fall 1998 was a consequence of both the LC and local forcing. The LC-induced flows and their bottom Ekman layer responses were necessary to transport properties from the shelf-break to the mid-shelf. The locally driven flows and their bottom Ekman layer responses (further amplified by the LC effect) then took over to transport properties to the near-shore. Moreover, the trajectory paths tend to intercept the near-shore region between Tampa Bay and Charlotte Harbor, consistent with the

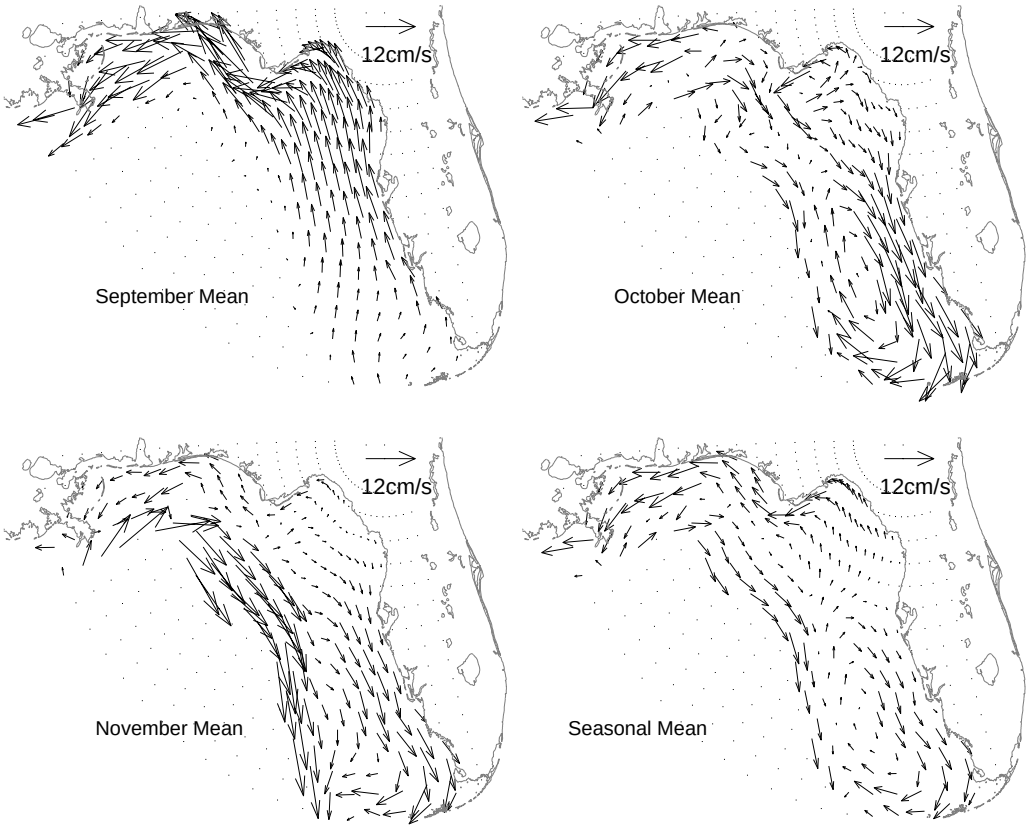

Fig. 11. Evolution of the monthly mean, depth averaged velocity vectors for September, October and November along with the fall 1998 seasonal mean for Case I.

local upwelling maximum argument advanced by Weisberg et al. (2000).

5. Scalar fields and temperature budget

5.1. Temperature and salinity fields

The combination of local plus LC forcing also affects the scalar fields of temperature and salinity. Figs. 14 and 15 show the modeled SST and sea surface salinity (SSS) fields at the end of the model run on November 30th for Cases I and II, respectively. Since the model is initialized in either case with spatially uniform SST and SSS, these figures show the relative effects of local and deep-water momentum and buoyancy fluxes in changing SST and SSS. Both sets of figures are similar in that SST is cooler and SSS is fresher near-shore. The SST distributions are largely accounted for by the net surface heat flux transition from warming to cooling in fall. Surface cooling causes convective mixing which, when combined with shoaling topography, produces a seaward directed SST gradient. Ocean circulation dynamics, through upwelling, is also a factor, and this accounts for the Case II SST being cooler ($\sim 1^{\circ}$C) than the Case I SST since relatively deeper, colder water is advected shoreward under Case II.

SSS shows less inter-case difference than SST. This is because low salinity derives from coastal river plumes advected by the near-shore flow fields that are very similar in both cases. However, the fall SSS fields differ markedly from their spring transition (HW02) counterparts. We attribute this to the change in seasonal average circulation from downwelling to upwelling to the west and east of Cape San Blas, respectively. As a result, waters of

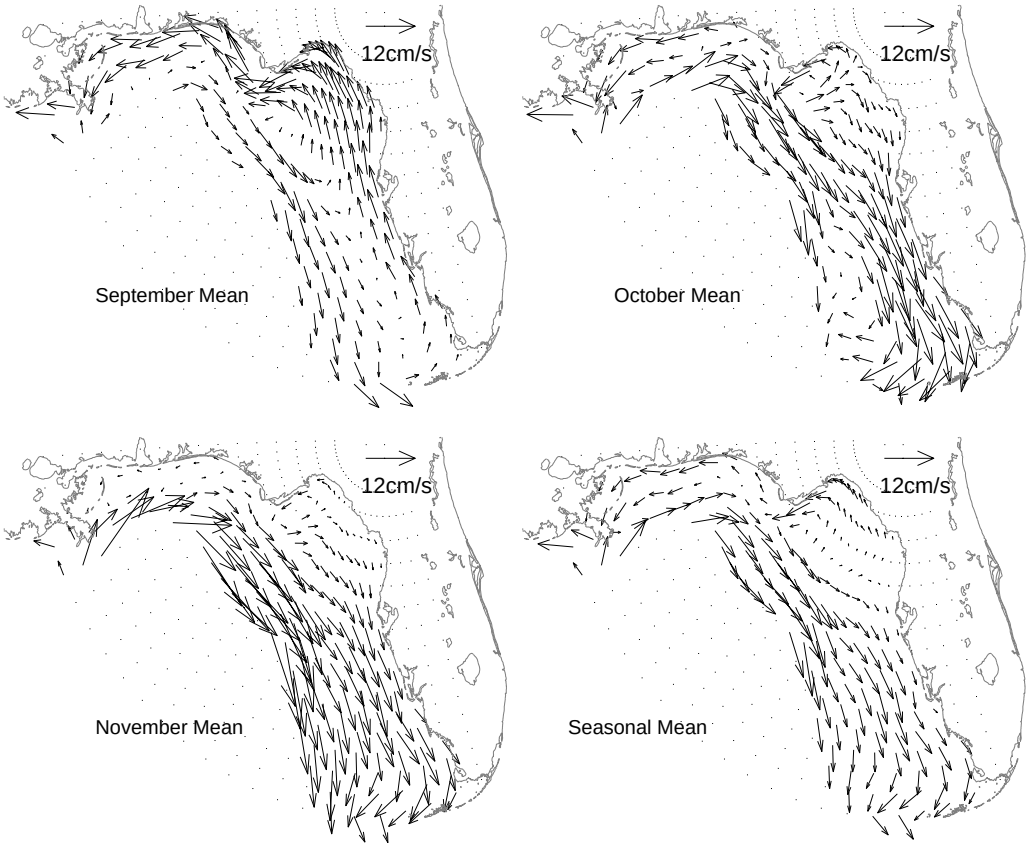

Fig. 12. Evolution of the monthly mean, depth averaged velocity vectors for September, October and November along with the fall 1998 seasonal mean for Case II.

Mississippi River, Mobile River, and Florida Panhandle origin are limited to the western part of the study region in fall, whereas they are advected southeastward in spring. This may be one reason why the "green river" phenomenon (Gilbes et al., 1996) occurs in spring and not in fall.

5.2. The temperature equation

The three-dimensional temperature budget for the fall 1998 transition is diagnosed in parallel to the HW02 spring 1999 analyses. The temperature equation is recast from its modeled flux divergence, σ-coordinate form (Blumberg and Mellor, 1987) to an advective, z-coordinate form. Thus, we diagnose

$$\frac{\partial T}{\partial t} = -u\frac{\partial T}{\partial x} - v\frac{\partial T}{\partial y} - w\frac{\partial T}{\partial z} + \frac{\partial}{\partial x}\left(A_H\frac{\partial T}{\partial x}\right) + \frac{\partial}{\partial y}\left(A_H\frac{\partial T}{\partial y}\right) + \frac{\partial}{\partial z}\left(K_H\frac{\partial T}{\partial Z}\right) \quad (1)$$

which equates the local rate of change of temperature($\partial T/\partial t$) to a combination of the flow field advective rate of change ($-u\partial T/\partial x - v\partial T/\partial y - w\partial T/\partial z$) and the rates of change by horizontal $[[\partial/\partial x(A_H\partial T/\partial x) + \partial/\partial y(A_H\partial T/\partial T)]]$ and vertical $[\partial/\partial z(K_H\partial T/\partial z)]$ diffusion. We diagnose the budget with respect to time series of both vertical averages and depth profiles at two different isobaths, and a seasonal mean across-shelf section.

The two time series analysis locations, A and B (see Fig. 1), are on the 50 m isobath in the Big Bend and the 15 m isobath offshore of Sarasota,

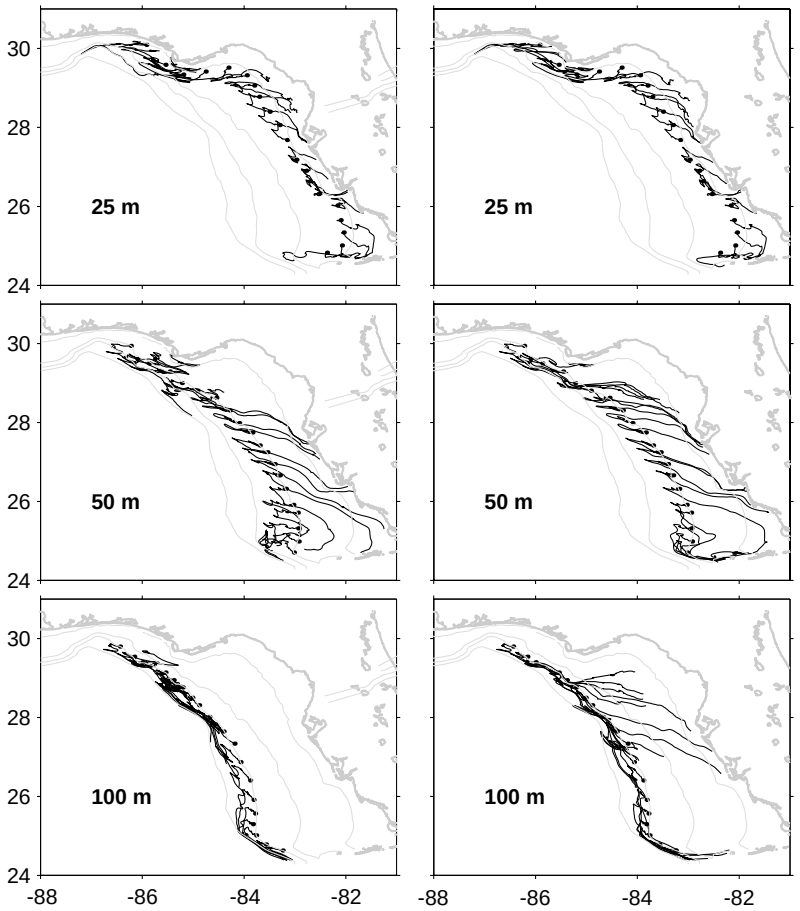

Fig. 13. Modeled Lagrangian trajectories tracked over three month of the drifters released along 25, 50, and 100 m isobath near the bottom. Left and right panels are for Cases I and II, respectively.

respectively. Through a term-by-term analysis of Eq. (1) we quantify the contributions by each physical process in changing temperature. For brevity we only consider Case II since comparisons between the modeled and observed temperature sections suggest that Case II is closer to reality than Case I. The differences in the temperature balances between these two cases are discussed in Section 5.5.

5.3. Depth-average balances

Vertically integrating Eq. (1) provides a depth-average temperature equation. Because horizontal diffusion is negligible the depth-average diffusion is essentially the depth-average vertical diffusion $[Q/(\rho C_P H)$, where Q is the net surface heat flux, ρ and C_P are the seawater density and specific heat, and H is the water depth]. Vertically integrated water column temperature variations thus depend on the surface heat flux and the heat flux divergence by the ocean circulation.

Time series of these two depth-average terms and their sum are shown for points A and B in Fig. 16. As an analysis check we note that the sum is nearly identical to the depth-average local rate of temperature change. Means and standard deviations are provided for each term to account for their relative contributions to the seasonal and synoptic scale variations, respectively.

The magnitudes of the advective and diffusive contributions are similar at the mid-shelf point A

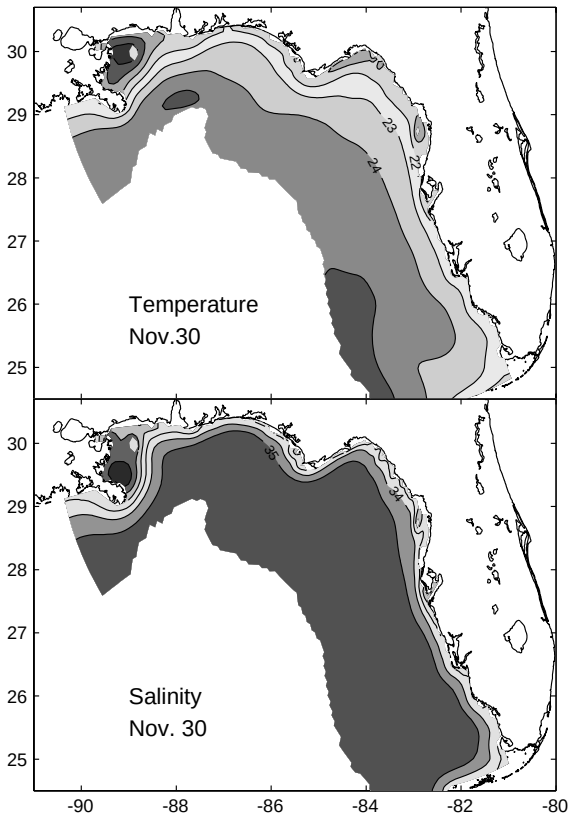

Fig. 14. Modeled (Case I) sea surface temperature and sea surface salinity fields at the end of fall 1998 model simulation (November 30, 1998).

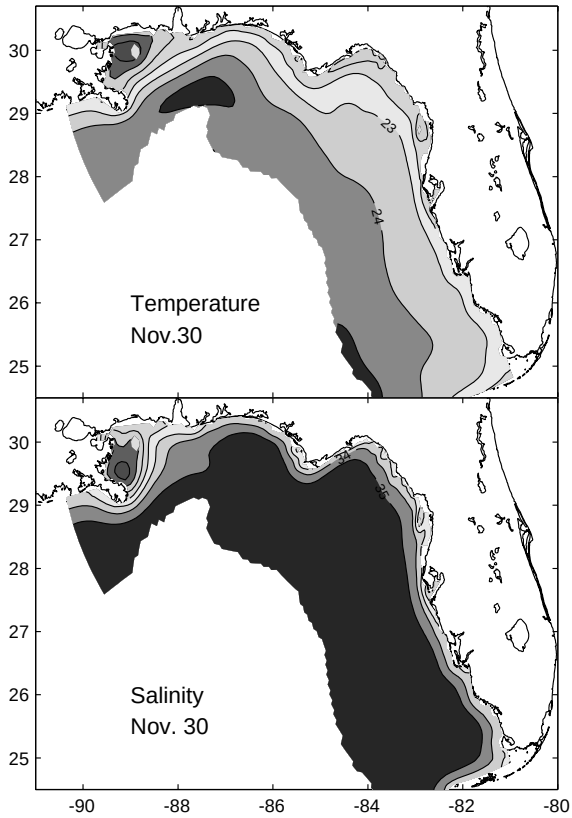

Fig. 15. Modeled (Case II) sea surface temperature and sea surface salinity fields at the end of fall 1998 model simulation (November 30, 1998).

location. The seasonal change (given by the three-month mean values), being negative (cooling), is primarily controlled by surface heat flux, whereas the synoptic variability (given by the standard deviations) relies on both surface heat flux and ocean advection. Interestingly, the ocean advection and surface heat flux terms tend to counteract one another mitigating temperature change over the first half of the season, whereas they add constructively over the second half. On seasonal average, advection enhances the total water column cooling (-4.16°) by about 15%. For the synoptic scale variability advection is slightly more effective than the surface heat flux in changing the water column temperature. The largest variations correspond to the three major storm events: Hurricanes Earl, Georges, and Mitch.

The relative importance between ocean advection and surface heat flux changes upon approaching shallow water. At point B, closer to the coast, the seasonal water column cooling (-6.90°) is almost entirely by surface heat flux, and surface heat flux also plays a larger role than ocean advection at synoptic scales. Thus, the shallower the water the larger the fall transition temperature change and the larger the role of surface heat flux over ocean advection. Advection does serve to mitigate change in an interesting way. Once a seaward temperature gradient is established, upwelling favorable wind events can lead to counter-intuitive warming as warmer offshore-located waters are advected and upwelled into the colder near-shore region.

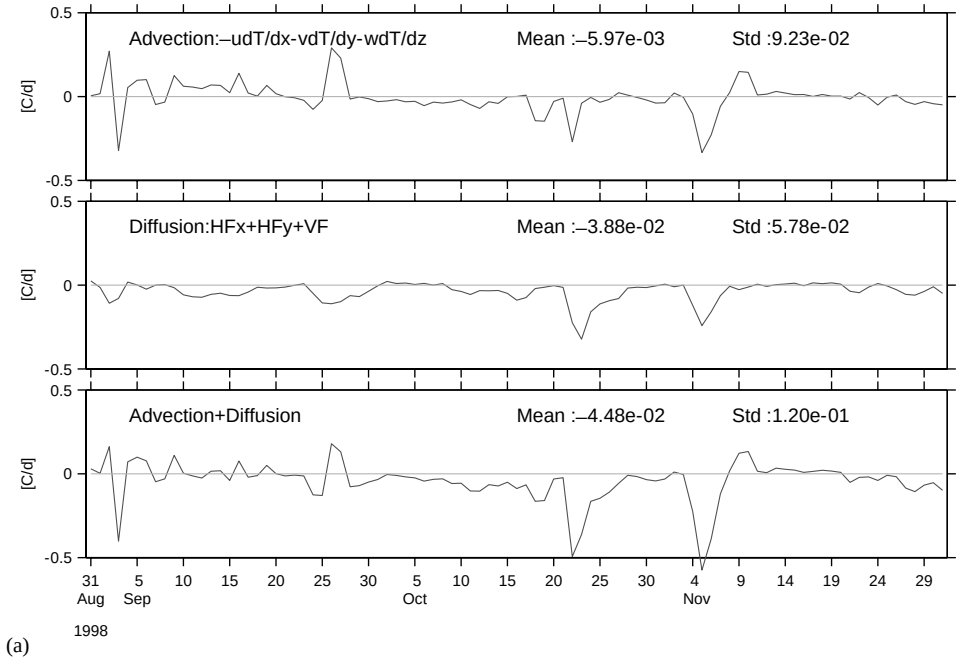

(a)

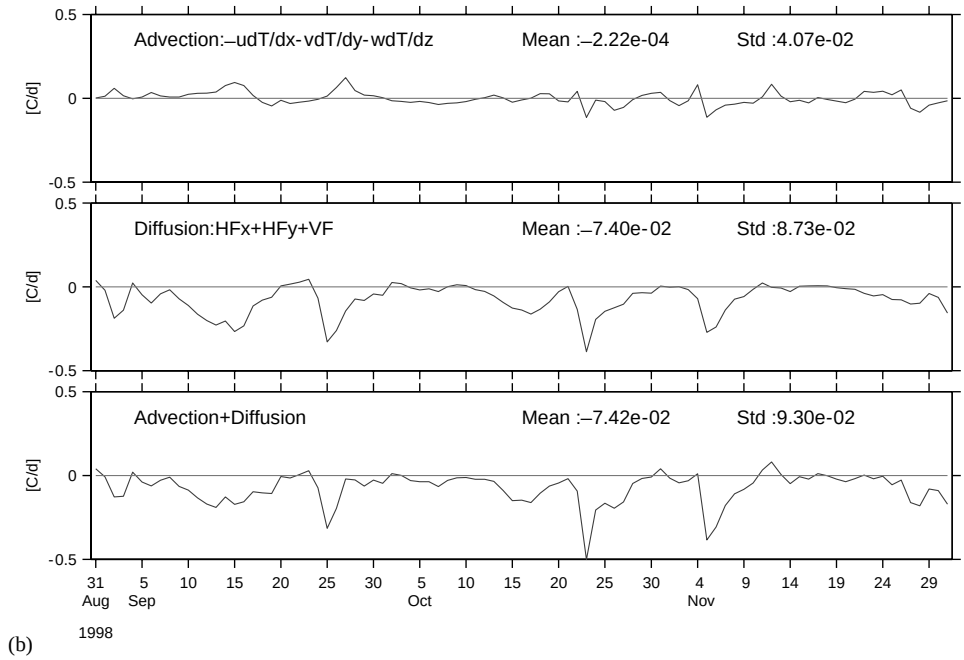

(b)

Fig. 16. (a) The relative contributions to the depth-averaged temperature balance by ocean circulation and diffusion at station A. Three time series are shown: the advection, the diffusion and their sum (which is nearly exactly equals the local change of depth-average temperature). Accompanying each time series are their seasonal means and standard deviations in units of $^{\circ}$C day^{-1} as measures of the seasonal and synoptic scale variability. (b) Same as (a), but for station B.

5.4. Vertical profiles of the term-by-term temperature balance

The temperature budget is further explored in Figs. 17a and b by a term-by-term analysis of the vertical structure of the temperature variability at points A and B, respectively. In each of these figures the left-hand panels show the horizontal and vertical components of the ocean advection and their sum, and the right-hand panels show the diffusion (primarily vertical), the diffusion plus the advection (nearly identical to the local rate of change of temperature), and the temperature itself. Shaded and clear contours are used to denote warming and cooling tendencies, respectively. Destratification, do to convective mixing in response to net surface cooling, distinguishes the fall from the spring transition when net surface heating leads to stratification (HW02). Convective mixing renders the vertical temperature gradient ($\partial T/\partial z$) smaller in fall than in spring so the contribution to the temperature budget by vertical advection ($w\partial T/\partial z$) in fall is less than in spring, especially in shallow water. Nevertheless, and depending on location, the role of ocean advection on both the synoptic and seasonal scales may be comparable to that of diffusion and oftentimes it is of opposite sign. As with spring, the thermodynamics are fully three-dimensional, and the omission of any of the coordinate directions would compromise a model's ability to describe the temperature evolution.

The balances at the deeper and shallower isobath stations show interesting evolution differences. At the 50 m isobath (Fig. 17a) we see that all of the terms are of comparable magnitude at synoptic scales. Initially, while the water column is stratified, advection tends toward warming at all depths while diffusion tends toward cooling near the surface. Upon addition, we see that the thermocline erodes due to the simultaneous cooling near-surface and warming at depth. Once the horizontal temperature gradient reverses from landward- to seaward-directed ocean advection by itself tends toward cooling near-surface and warming at depth. This is evident at the shallow water location B (Fig. 17b). The predominantly upwelling favorable circulation of fall 1998 then advects cooler water seaward near the surface and warmer water shoreward at depth. The opposite tendency is mirrored in the diffusion term as convective mixing is driven from both above and below. Such mixing tends to warm near the surface (despite negative surface heat flux) and cool at depth. The net result is a nearly vertically uniform temperature that decreases monotonically from fall to winter.

The counter-intuitive result of the ocean advection not only provides for more effective mixing (from below in addition to from above); it also leads to a positive feedback that increases the net surface heat flux from the ocean to the atmosphere locally. It does this by replenishing the near surface with relatively warmer water from below than would exist in the absence of advection. Ocean advection therefore lengthens the fall season transition nearshore.

5.5. Across-shelf transects for the seasonal mean temperature budget

Here we compare the fall 1998 Cases I and II seasonal mean temperature budgets with that for spring 1999 (HW02) relative to an across-shelf section offshore of Sarasota (Fig. 1). The purposes are to illustrate the relative effects of local versus LC forcing in fall 1998 and the differences between the fall and spring transitions. Seasonal mean ocean advection, diffusion, and their sum are shown in Fig. 18 where seasonal means of each of these terms are obtained by averaging the model-diagnosed temperature budget from September 1st to November 30th for fall 1998 and from March 1st to May 31st for spring 1999.

Consider first the relative balances in fall 1998 between the local forcing only and local plus LC forcing, Cases I and II, respectively. Near-shore the two cases are nearly identical. Upwelling on seasonal average provides tendencies for warming (cooling) near the bottom (surface) for the non-intuitive reasons explained earlier. Diffusion on seasonal average provides a cooling which exceeds the magnitude of the advective warming. The net result is near-shore cooling over the entire water column. The effects of the LC are seen most clearly at mid-shelf and seaward, especially over the lower

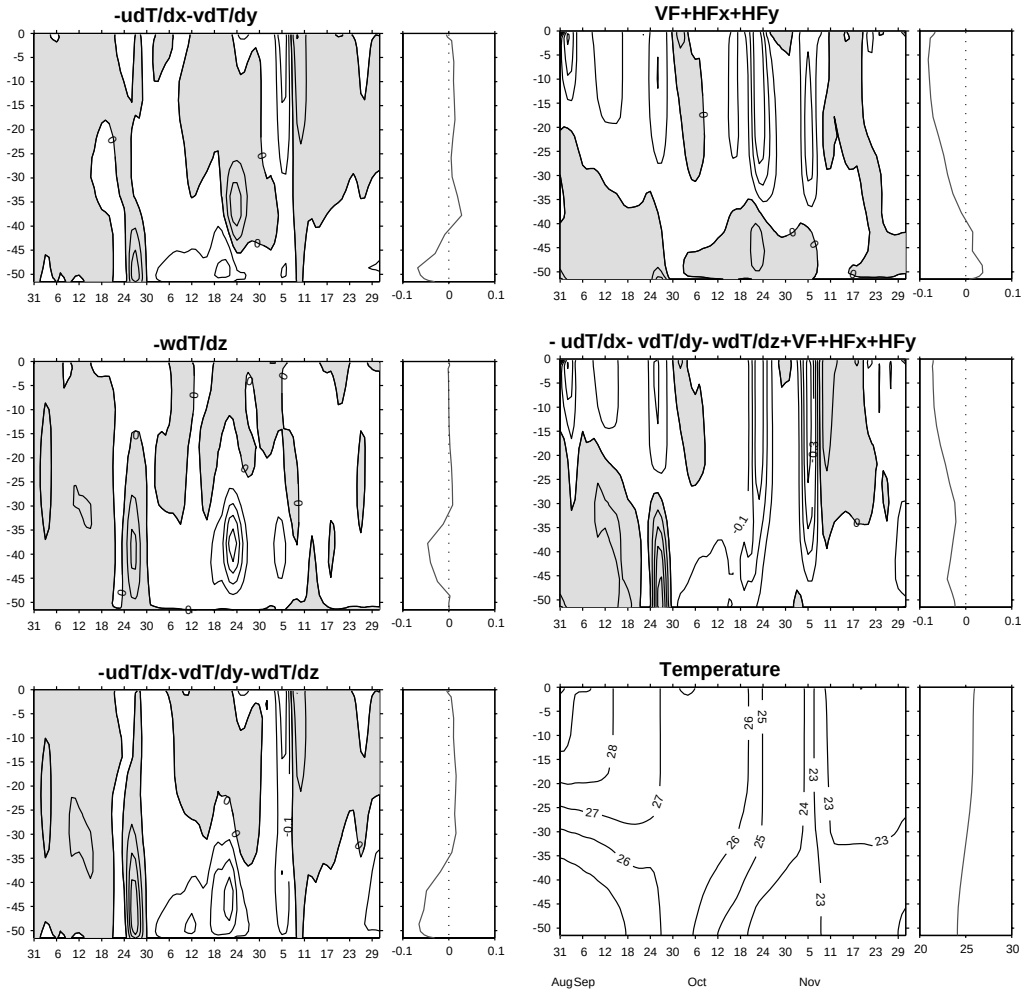

(a)

Fig. 17. (a) Time series of the depth profiles of the individual terms that compose the temperature balance at Station A. The left-hand panels show the horizontal and vertical components of the ocean advection and their sum, and the right-hand panels show the diffusion, the diffusion plus the advection, and the temperature. To the right of each panel is the seasonal mean profile. The contour interval for each of the budget term is $0.1^{\circ}\mathrm{C\,day^{-1}}$, and the contour interval for temperature is $1^{\circ}\mathrm{C}$. Shading indicates warming and clear indicants cooling. (b) Same as (a), but for station B.

portion of the water column. There, enhanced across-shelf transport and upwelling of cold, deep-water (e.g., Fig. 9) leads to enhanced cooling over the entire shelf. In either of the fall cases, despite counteracting advective and diffusive influences over some portions of the domain, cooling wins out over the upper ocean (depths less than 40 m in Case I and at all depths shown in Case II).

The spring 1999 seasonal average balances differ from either of the fall 1998 cases in that advection and diffusion tend to add constructively almost everywhere. Also the seasonal mean temperature advection tendency in spring 1999 is smaller in magnitude than the advection tendencies under either of the fall 1998 cases. These fundamental differences between the fall and spring transitions are attributed to three factors. The first is the opposite changes in state from destratified to stratified conditions in spring versus stratified to destratified conditions in fall. The second is the

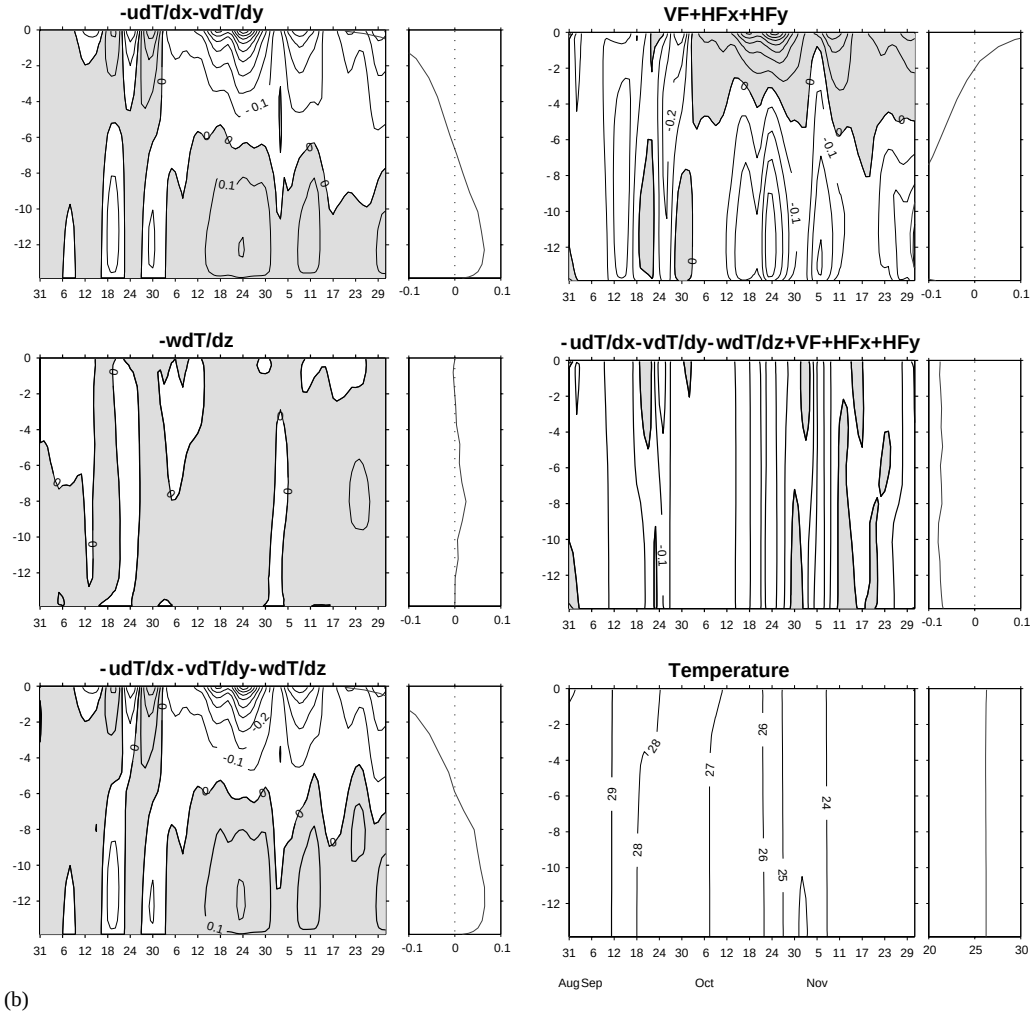

(b)

Fig. 17 (*continued*).

predominantly upwelling conditions in fall 1998 leading to an increased circulation dynamics influence over that in spring 1999. In other words, both the temperature gradients and the currents are persistently larger in fall 1998 than in spring 1999 leading to a relatively larger advective influence. The third factor entails the counter-intuitive finding of upwelling leading to near-shore warming in fall, which does not occur in spring when the temperature gradient is directed land-ward. Our results are consistent with the North Carolina coast results of Austin (1999) in that surface heat flux and ocean advection are both important. However, here the thermodynamics are fully three-dimensional, spatially inhomogeneous, and dependent on both local and deep-ocean forcing influences.

6. Summary and conclusions

Mid-latitude continental shelves undergo a fall transition as the net surface heat flux changes from warming to cooling. Using in situ data and a numerical circulation model, we investigate the circulation and temperature budget on the WFS

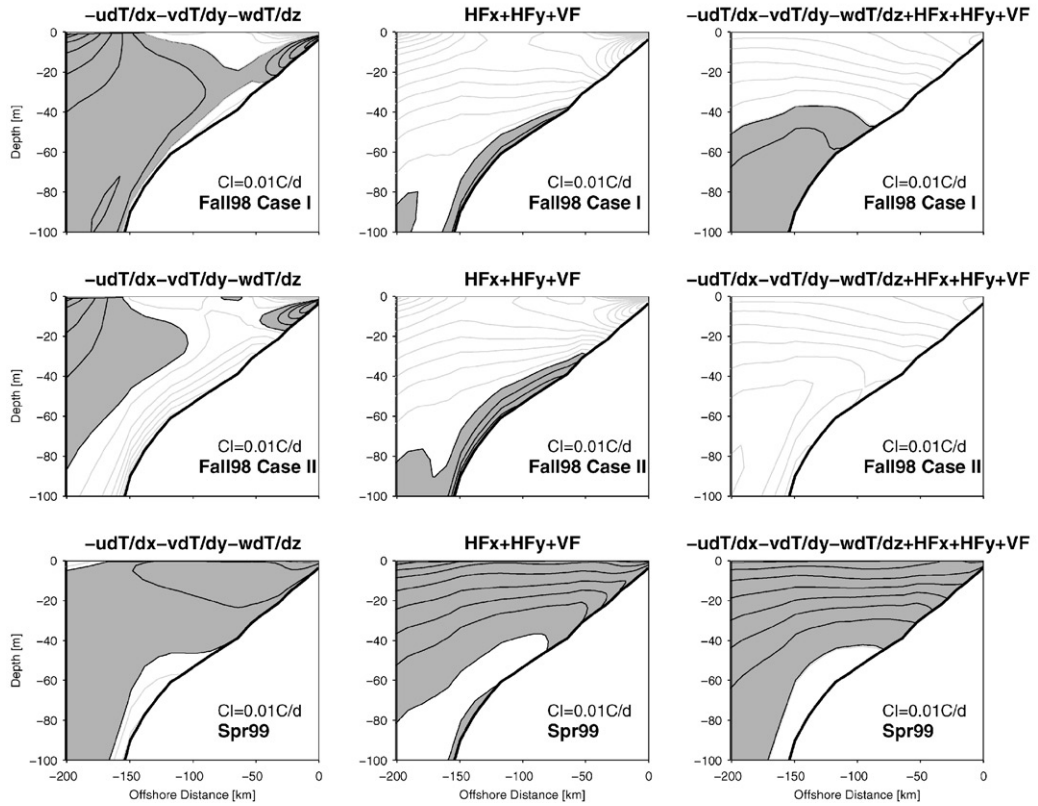

Fig. 18. Across-shelf transect (off Sarasota, FL) profiles of seasonal means of ocean advection (left panels), diffusion terms (middle panels) and their sums (right panels) for Fall 98 Case I (upper panels), Fall 98 Case II (middle panels) and Spring 99 (lower panels). The contour interval is indicated in each panel. The shading and clear contour denote warming and cooling effects, respectively.

for the fall transition of 1998. The data consist of sea level from coastal stations and velocity profiles from instruments moored between the 25 m and the 10 m isobaths. The model is a regional adaptation of the primitive equation, POM forced by NCEP reanalysis wind stress, air pressure, and heat flux fields and by river inflows. By running twin experiments, one by local forcing only and the other by both local forcing and an idealized LC effect, we investigate the relative importance of local and deep-ocean forcing in affecting the shelf circulation. Based on comparisons with observations we conclude that the inner-shelf circulation primarily occurs in response to local forcing.

Remote forcing by the LC (as occurred in fall 1998) does have important effects, nevertheless. Distinctive differences between two cases are found over the middle to outer portions of the shelf. By intensifying the mid-shelf currents the LC influence leads to a stronger on-shore transport within the bottom Ekman layer. Lagrangian particle tracking over the three month fall season with and without the LC influence shows that the LC is instrumental in causing cold, nutrient-rich water of deep-ocean origin to be transported between the shelf-break and the inner-shelf. Such increased bottom Ekman layer transport is responsible for the elevated primary productivity that occurred in fall 1998 (Walsh et al., 2003). While ecologically significant, such remote LC interactions appear to be rare. Of the 10 years of TOPEX/Poseidon altimetry records examined by Weisberg and He (2003) such events only occurred in two of these years (1997 and 1998).

Measurements on the WFS suggest a seasonal cycle in which the circulation tends toward

upwelling in winter and downwelling in summer. Between these two phases are the spring and fall transitions due to the sign changes in the net surface heat flux. Weisberg et al. (1996) hypothesized that the circulations observed during the seasonal transitions are due in part to the baroclinicity imposed by surface heat flux. The present (fall transition) study together with HW02 (spring transition) confirm this hypothesis. Due to the combined effects of surface heat flux and shoaling topography, the across-shelf temperature gradient ($\partial T/\partial x$)changes direction from seaward (landward) to landward (seaward) during the spring (fall) transition, and the associated baroclinic circulation flows northwestward (southeastward). Such baroclinic circulation, adding either constructively or destructively to the wind-driven circulation, provides both season and location-dependent along and across-shelf current distributions.

Through a three-dimensional, term-by-term analysis of the temperature budget, we describe the evolution of the WFS temperature in the fall season as a complement to the HW02 spring analyses. The WFS temperature balance has distinctive seasonal variations. Through a depth-average temperature analysis, we find that surface heat flux controls the temperature variations for both the seasonal and synoptic scales in fall. This differs from spring when surface heat flux and ocean advection control the temperature variations on seasonal and synoptic scales, respectively (HW02). The shallower the water, the larger the fall transition temperature change, and the larger the relative role of surface heat flux over ocean advection.

Net surface cooling in fall leads to convective mixing that rapidly alters the temperature gradient. A counter-intuitive consequence, revealed by analyzing the depth dependence of the temperature budget, is that upwelling can cause warming (cooling) near the bottom (the surface) as warmer (cooler) water is transported landward (seaward) at depth (the surface). Over the inner-shelf the tendency for temperature diffusion and advection to offset each other throughout the water column results in a nearly vertically uniform (and negative) local rate of temperature change that leads to destratification in fall. Similar to the spring transition, the WFS temperature balances are complex and fully three-dimensional. A corollary statement applies to all other ecologically important water properties.

Acknowledgements

This work was supported by grants from the Office of Naval Research, grant No. N00014-98-1-0158 and the National Oceanic and Atmospheric Administration, grant No. NA76RG0463. We benefited from an evolving program previously supported by the United States Geological Survey, the Minerals Management Service, and from an ongoing State of Florida, Coastal Ocean Monitoring and Prediction System (COMPS). Special thanks are offered to the family of Elsie and William Knight for the research fellowship endowment that helps to support R. He. Ocean Circulation Group staff (Messrs. R. Cole, J. Donovan, C. Merz, P. Smith) contributed to the field work and analyses. We thank F. Muller-Karger for providing assistance with the monthly mean SST fields. NCEP reanalysis fields were provided by NOAA-CIRES, Climate Diagnostics Center, Boulder, CO and obtained from their web site at http://www.cdc.noaa.gov/. This is ECOHAB contribution number 58.

References

Austin, J.A., 1999. The role of the alongshore wind stress in the heat balance of the north Carolina inner shelf. Journal of Geophysical Research 104, 18187–18203.

Blumberg, A.F., Mellor, G.L., 1987. A description of a three-dimensional coastal ocean circulation model. In: Heaps, N. (Ed.), Three-Dimensional Coastal Ocean Models, Vol. 4, AGU, Washington, DC. pp. 208–233.

Chu, P., Edmons, N., Fan, C., 1999. Dynamical mechanisms for the south china sea seasonal circulation and thermohaline varibilities. Journal of Physical Oceanography 29, 2971–2989.

Dever, E., Lentz, S.J., 1994. Heat and salt balances over the northern California shelf in winter and spring. Journal of Geophysical Research 99, 1001–16017.

Ezer, T., Mellor, G., 1992. A numerical study of the variability and separation of the Gulf stream, induced by surface

atmospheric forcing and lateral boundary flows. Journal of Physical Oceanography 22, 660–682.

Gilbers, F., Thomas, C., Walsh, J.J., Muller-Karger, F.E., 1996. An episodic chlorophyll plume on the West Florida Shelf. Continental Self Research 16, 1201–1224.

Gill, A.E., 1982. Atmosphere-Ocean Dynamics. Academic Press.

He, R., Weisberg, R.H., 2002a. West Florida shelf circulation and temperature budget for the 1999 spring transition. Continental Shelf Research 22 (5), 719–748.

He, R., Weisberg, R.H., 2002b. Tides on the west Florida shelf. Journal of Physical Oceanography 32 (12), 3455–3473.

He, R., Weisberg R, H., 2003. A Loop Current intrusion case study on the West Florida shelf. Journal of Physical Oceanography 33 (2), 465–477.

Hetland, R.D., Hsueh, Y., Leben, R.R., Niiler, P.P., 1999. A loop current induced jet along the edge of the west Florida shelf. Geophysical Reserch Letters 26, 2239–2242.

Kourafalou, V.H., Oey L, -Y., Wang J, D., Lee, T.L., 1996. The fate of river discharge on the continental shelf 1: Modeling the river plume and the inner shelf coastal current. Journal of Geophysical Research 101, 3415–3434.

Kundu, P.K, 1976. An analysis of inertial oscillations observed near the Oregon coast. Journal of Physical Oceanography 6, 879–893.

Lentz, S.J., 1987. A heat budget for the northern California shelf during the coastal ocean dynamics experiment. Journal of Geophysical Research 92, 14491–14509.

Lentz, S.J., Chapman D, .C., 1989. Seasonal difference in the current and temperature variability over the northern California shelf during the coastal ocean dynamics experiment. Journal of Geophysical Research 94, 12571–12592.

Marmorino, G.O., 1982. Wind-forced sea level variability along the west Florida shelf (winter, 1978). Journal of Physical Oceanography 12, 389–405.

Meyers, S.D., Siegel, E.M., Weisberg, R.H., 2000. Observation of currents on the west Florida shelf. Geophysical Research Letters 28 (10), 2037–2040.

Mellor, G.L., Yamada, T., 1982. Development of a turbulence closure model for geophysical fluid problems. Review Geophysics 20, 851–875.

Nowlin, W.D., Jochens, A.E., Howard, M.K., DiMarco, S.F., Schroeder, W.W., 2000. Hydrographic properties and inferred circulation over the northeast shelves of the Gulf of Mexico during spring to midsummer of 1998. Gulf of Mexico Science 18, 40–54.

Orlanski, I., 1976. A simple boundary condition for unbounded hyperbolic flows. Journal of Computational Physics 21, 251–269.

Pullen, J.D., 2000. Modeling studies of the coastal circulation off northern California, Ph.D. Dissertation, Oregon State University.

Smagorinsky, J., 1963. General circulation experiments with primitive equations I: the basic experiment. Monthly Weather Review 91, 99–164.

Walsh, J.J., Weisberg, R.H., Dieterle, D.A., He, R., Darrow, B.P., Jolliff, J.K., Lester, K.M., Vargo, G., Kirkpatrick, G.J., Fanning, K.A., Sutton, T.T., Jochens, A.E., Giggs, D.C., Nababan, B., Hu, C., Muller-Karger, F.E., 2003. The phytoplankton response to intrusion of slope water on the west Florida shelf: model and observations. Journal of Geophysical Research, in press.

Weisberg, R.H, Black, B.D., Yang, H., 1996. Seasonal modulation of the west Florida continental shelf circulation. Geophysical Research Letters 23, 2247–2250.

Weisberg, R.H., Black, B.D., Li, Z., 2000. An upwelling case study on the Florida west coast. Journal of Geophysical Research 105 (C5), 11459–11469.

Weisberg, R.H., Li, Z., Muller-Karger, F., 2001. West Florida shelf response to local wind forcing: April 1998. Journal of Geophysical Research 106 (C12), 31239–31262.

Weisberg, R.H., He, R., 2003. Local and deep-ocean forcing contribution to anomalous water properties on the west Florida shelf. Journal of Geophysical Research, in press.

Yang, H., Weisberg, R.H., Niller, P.P., Sturges, W., Johnson, W., 1999. Lagrangian circulation and forbidden zone on the west Florida shelf. Continental Shelf Research 19 (9), 1221–1245.